

Superfluid $^3\text{He-A}$ has domain-wall-like structures, which are called solitons. We calculate numerically the structure of a splay soliton. We study the effect of solitons on the nuclear-magnetic-resonance spectrum by calculating the frequency shifts and the amplitudes of the soliton peaks for both longitudinal and transverse oscillations of magnetization. The effect of dissipation caused by normal-superfluid conversion and spin diffusion is calculated. The calculations are in good agreement with experiments, except a problem in the transverse resonance frequency of the splay soliton or in magnetic-field dependence of reduced resonance frequencies.

PACS numbers: 67.57.Fg, 67.57.Lm

I. INTRODUCTION

Nuclear magnetic resonance (NMR) has turned out to be very useful for studying the superfluid phases of liquid ^3He . The two superfluid phases A and B are distinguished in the NMR spectrum by different frequency shifts of the absorption peaks.¹ In addition to these “bulk” peaks, one often observes additional “satellite” peaks. These are caused by topological objects and textures that appear in the superfluid order parameter. Especially in superfluid $^3\text{He-A}$, several different objects have been identified based on the frequency shifts of the satellite peaks.^{2,3,4} The simplest of these are solitons. They are domain-wall-like structures where a planar object separates two different but degenerate bulk states.

The satellite peaks in $^3\text{He-A}$ were first observed in measurements in the mid 1970's.^{5,6} Soon after the theory of solitons in ^3He was developed by Maki and Kumar.^{7,8} Their calculation gave a striking agreement with the measured frequency shifts of the satellite peaks at temperatures close to the superfluid transition temperature T_c . This initial success had the consequence that further studies of solitons went to other directions^{9,10,11,12} and, unfortunately, no more precise calculations were done.

A soliton has two basic structures, “twist” and “splay,” which correspond to the cases of a magnetic field ($B \gg 1$ mT) perpendicular and parallel, respectively, to the plane of the soliton wall. Both these structures can be studied using small oscillations of the magnetization that are either transverse or longitudinal relative to the static field.

There are several points that can be improved in the previous calculations, given as follows. (i) The structure of the splay soliton was calculated only by using variational approximation. (ii) The calculations were limited to temperatures near T_c . (iii) The effect of different parameter values was not studied. (iv) The amplitudes and widths of the satellite peaks as well as peaks of higher order were not studied. (v) Dissipation was neglected. It is just these points that we address in this paper. An additional motivation is that the study of solitons opens the way to detailed understanding of more complicated topological objects such as vortices.

We find that, using dissipationless theory, the agreement between the theoretical and experimental frequency shifts is generally very good. However, we find a puzzling disagreement in the transverse oscillation frequency of the splay soliton. This disagreement has remained unnoticed because no detailed comparison between theory and experiment has been published. Further, we find that the theory is particularly inflexible to explain this discrepancy away. Taking into account dissipation, in particular spin diffusion, changes these conclusions. On one hand, the disagreement in the splay-soliton frequency is reduced. On the other hand, we find considerable extra shift of resonance frequencies in high fields, which has not been reported experimentally. We also point out that the longitudinal resonance of the splay soliton has not been studied experimentally. Measurement of these quantities would be important to test our understanding of the basic properties of superfluid ^3He .

We start in Sec. II with a short introduction to the hydrodynamic theory and NMR in $^3\text{He-A}$. In Sec. III we solve numerically the structure of the splay soliton. The frequency and the absorption of the principal satellite peak are determined in Secs. IV and V ignoring dissipative effects. In Sec. V we calculate the frequencies and absorption of the higher modes. In Sec. VI we take into account dissipation and calculate the effect of the spin diffusion and normal-superfluid relaxation on the absorption spectrum.

Here we briefly present some main points of the hydrodynamic theory and NMR in $^3\text{He-A}$. The order parameter of superfluid $^3\text{He-A}$ is a 3×3 tensor of the form^{2,13}

$$A_{\mu j} = \Delta \hat{d}_\mu (\hat{m}_j + i \hat{n}_j), \quad (1)$$

where $\hat{\mathbf{d}}$, $\hat{\mathbf{m}}$ and $\hat{\mathbf{n}}$ are unit vectors and $\hat{\mathbf{m}} \perp \hat{\mathbf{n}}$. It is conventional to define $\hat{\mathbf{l}} = \hat{\mathbf{m}} \times \hat{\mathbf{n}}$, which gives the axis of the orbital angular momentum of a Cooper pair. The unit vector $\hat{\mathbf{d}}$ defines the axis along which the spin of the Cooper pair vanishes. In a static magnetic field, the structure of a soliton can be determined by finding a local minimum for the free energy^{2,14,15}

$$F_{\text{static}} = \int d^3r (f_d + f_g + f_h). \quad (2)$$

Here f_d comes from the dipole-dipole interaction between nuclear moments,

$$f_d = -\frac{1}{2} \lambda_d (\hat{\mathbf{d}} \cdot \hat{\mathbf{l}})^2, \quad (3)$$

f_h from coupling to the external field \mathbf{B} ,

$$f_h = \frac{1}{2} \lambda_h (\hat{\mathbf{d}} \cdot \mathbf{B})^2, \quad (4)$$

and f_g from the gradient of the order parameter,

$$\begin{aligned} 2f_g = & \rho_\perp \mathbf{v}_s^2 + (\rho_\parallel - \rho_\perp) (\hat{\mathbf{l}} \cdot \mathbf{v}_s)^2 + 2C \mathbf{v}_s \cdot \nabla \times \hat{\mathbf{l}} \\ & - 2C_0 (\hat{\mathbf{l}} \cdot \mathbf{v}_s) (\hat{\mathbf{l}} \cdot \nabla \times \hat{\mathbf{l}}) + K_s (\nabla \cdot \hat{\mathbf{l}})^2 + K_t (\hat{\mathbf{l}} \cdot \nabla \times \hat{\mathbf{l}})^2 \\ & + K_b |\hat{\mathbf{l}} \times (\nabla \times \hat{\mathbf{l}})|^2 + K_5 |(\hat{\mathbf{l}} \cdot \nabla) \hat{\mathbf{d}}|^2 + K_6 \sum_{i,j} [(\hat{\mathbf{l}} \times \nabla)_i \hat{d}_j]^2. \end{aligned} \quad (5)$$

The gradient energy (5) also includes the kinetic energy arising from the superfluid velocity $\mathbf{v}_s = (\hbar/2m_3) \sum_i \hat{m}_i \nabla \hat{n}_i$, where m_3 is the mass of a ^3He atom. However, in the following we limit to the case of zero superfluid velocity. The parameters appearing in the gradient energy have been calculated in the weak-coupling approximation by Cross¹⁴ and Dörfle,¹⁶ the latter including more Fermi-liquid parameters. For numerical values see Refs. 17 and 18. The characteristic scales are given by the dipole length $\xi_d = (\hbar/2m_3) \sqrt{\rho_\parallel / \lambda_d} \approx 10 \text{ } \mu\text{m}$ and the dipole field $B_d = \sqrt{\lambda_d / \lambda_h} \approx 2 \text{ mT}$.

We consider a static field $\mathbf{B}_0 = B_0 \hat{\mathbf{z}}$. We assume that the equilibrium $\hat{\mathbf{d}}$, denoted by $\hat{\mathbf{d}}_0$, lies in the plane perpendicular to \mathbf{B}_0 :

$$\hat{\mathbf{d}}_0 = \hat{\mathbf{x}} \cos \theta + \hat{\mathbf{y}} \sin \theta. \quad (6)$$

This situation is always achieved in large field $B_0 \gg B_d$, where $\hat{\mathbf{d}}$ is forced to the plane by f_h (4), but in some cases this happens in low fields as well. Minimization of the total energy (2) gives for θ the equation

$$\mathcal{D}\theta + (\hat{\mathbf{l}} \cdot \hat{\mathbf{d}}_0) (\hat{\mathbf{l}} \times \hat{\mathbf{d}}_0)_z = 0, \quad (7)$$

where the operator \mathcal{D} is defined by

$$\mathcal{D}f = -\frac{K_6}{\lambda_d} \nabla^2 f - \frac{K_5 - K_6}{\lambda_d} \nabla \cdot [\hat{\mathbf{l}} (\hat{\mathbf{l}} \cdot \nabla) f]. \quad (8)$$

In a dynamic magnetic state one has to include the spin magnetization $\gamma \mathbf{S}$ as a new variable in addition to $\hat{\mathbf{d}}$ and $\hat{\mathbf{l}}$. The effective energy density has the form^{1,2}

$$f_{\text{eff}} = \frac{\mu_0 \gamma^2}{2} \mathbf{S} \cdot \overset{\leftrightarrow}{\chi}^{-1} \cdot \mathbf{S} - \gamma \mathbf{S} \cdot \mathbf{B} + f_d + f_g, \quad (9)$$

where γ is the gyromagnetic ratio and $\vec{\chi}$ the susceptibility tensor. This leads to the equations of motion

$$\dot{\mathbf{S}} = \gamma \mathbf{S} \times \mathbf{B} - \hat{\mathbf{d}} \times \frac{\delta f}{\delta \hat{\mathbf{d}}}, \quad (10a)$$

$$\dot{\hat{\mathbf{d}}} = \hat{\mathbf{d}} \times \gamma \left(\mathbf{B} - \frac{\mu_0 \gamma}{\chi} \mathbf{S} \right), \quad (10b)$$

where $f = f_d + f_g$ and χ is the susceptibility in the normal state. The motion of $\hat{\mathbf{l}}$ is strongly limited by viscosity and therefore we assume that $\hat{\mathbf{l}}$ is independent of time.¹⁹ Equations (10) describe dissipationless dynamics. The inclusion of dissipative terms is postponed to Sec. VI. The field \mathbf{B} is the sum of the static field \mathbf{B}_0 and a small radio-frequency field \mathbf{B}' that oscillates at angular frequency ω . Throughout this paper we limit to study the linear response of \mathbf{S} and $\hat{\mathbf{d}}$ to \mathbf{B}' . We parametrize the deviation of $\hat{\mathbf{d}}$ with two parameters d_θ and d_z ,

$$\hat{\mathbf{d}} = \hat{\mathbf{d}}_0 + (\hat{\mathbf{z}} \times \hat{\mathbf{d}}_0) d_\theta + \hat{\mathbf{z}} d_z. \quad (11)$$

For \mathbf{S} we parametrize the deviation \mathbf{S}' from the equilibrium $\mathbf{S}_0 = \chi \mathbf{B}_0 / \mu_0 \gamma$ by $S'_z = S_z - S_0$ and circular components $S^\pm = S_x \pm i S_y$. Similar definitions are used for other vectors as well. We linearize Eqs. (10) and assume the time dependence $\mathbf{S}'(t) = \mathbf{S}' \exp(-i\omega t)$, etc. Using the equilibrium condition (7) we get

$$\omega S^\pm = \pm \omega_0 S^\pm \mp \lambda_d e^{\pm i\theta} (\mathcal{D} + U_\perp) d_z + i \lambda_d e^{\pm 2i\theta} l_z l_\mp d_\theta \mp \chi B_0 B_\pm, \quad (12a)$$

$$\omega d_z = \frac{\mu_0 \gamma^2}{2\chi} (S^- e^{i\theta} - S^+ e^{-i\theta}) + \frac{\gamma}{2} (B_+ e^{-i\theta} - B_- e^{i\theta}), \quad (12b)$$

$$\omega S'_z = -i \lambda_d (\mathcal{D} + U_\parallel) d_\theta + i \lambda_d (\hat{\mathbf{d}}_0 \times \hat{\mathbf{l}})_z l_z d_z, \quad (12c)$$

$$\omega d_\theta = i \frac{\mu_0 \gamma^2}{\chi} S'_z - i \gamma B'_z. \quad (12d)$$

Here $\omega_0 = \gamma B_0$ is the Larmor frequency. The potentials U_\parallel and U_\perp are defined by

$$U_\parallel = 1 - l_z^2 - 2(\hat{\mathbf{l}} \times \hat{\mathbf{d}}_0)_z^2 \quad (13)$$

$$U_\perp = 1 - 2l_z^2 - (\hat{\mathbf{l}} \times \hat{\mathbf{d}}_0)_z^2 - \frac{K_6}{\lambda_d} (\nabla \theta)^2 - \frac{K_5 - K_6}{\lambda_d} (\hat{\mathbf{l}} \cdot \nabla \theta)^2. \quad (14)$$

In order to simplify Eqs. (12), let us consider the special case $l_z \equiv 0$. In this case the equations separate into independent blocks for longitudinal and transverse oscillations of the magnetization. The resonance frequencies are determined by two independent Schrödinger-type equations for d_θ and d_z ,

$$(\mathcal{D} + U_\parallel) d_\theta = \alpha_\parallel d_\theta, \quad (15)$$

$$(\mathcal{D} + U_\perp) d_z = \alpha_\perp d_z. \quad (16)$$

The eigenvalues $\alpha_{\parallel,k}$ and $\alpha_{\perp,k}$ of these equations are related to the resonance frequencies as

$$\omega_{\parallel,k}^2 = \Omega^2 \alpha_{\parallel,k}, \quad (17)$$

$$\omega_{\perp,k}^2 = \omega_0^2 + \Omega^2 \alpha_{\perp,k}. \quad (18)$$

Here $\Omega = (\mu_0 \gamma^2 \lambda_d / \chi)^{1/2}$ is the longitudinal resonance frequency of the A phase. The corresponding eigenfunctions of Eqs. (15) and (16) are denoted by $\psi_{\parallel,k}$ and $\psi_{\perp,k}$, respectively. They are assumed to be normalized: $\int d^3 r |\psi_{\parallel,k}|^2 = 1$ and $\int d^3 r |\psi_{\perp,k}|^2 = 1$. Because we have temporarily neglected dissipative processes, the power absorption $P(\omega)$ consists of δ -peaks, $P(\omega) = \sum_k I_k \delta(\omega - \omega_k)$.

Instead of assuming $l_z \equiv 0$, an alternative approach to Eqs. (12) is to study the high-field limit $\omega_0 \gg \Omega$. More precisely, one can calculate the resonance frequencies as a power series of Ω^2 and neglect terms of the order of Ω^4 and higher. In this approximation all the three components S'_z , S^+ , and S^- decouple. The eigenvalue equations and frequencies are the same as above equations (15)-(18) except that Eq. (18) is valid only to leading order in Ω :

$$\omega_{\perp,k} = \pm \left[\omega_0 + \frac{\Omega^2}{2\omega_0} \alpha_{\perp,k} + O\left(\frac{\Omega^4}{\omega_0^3}\right) \right]. \quad (19)$$

For the rest of this section we assume the high-field limit $\omega_0 \gg \Omega$.

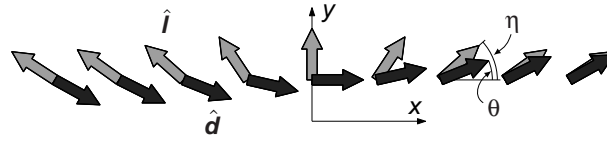


FIG. 1: The structure of a splay soliton, where the $\hat{\mathbf{l}}$ field (light arrows) has splay shape. The structure is homogeneous in the y - z plane of the soliton wall. Both $\hat{\mathbf{d}}$ and $\hat{\mathbf{l}}$ are perpendicular to the static field $\mathbf{B}_0 = B_0 \hat{\mathbf{z}}$.

In the case of dipole locking, $\hat{\mathbf{l}}(\mathbf{r}) = \hat{\mathbf{d}}(\mathbf{r})$, the lowest bulk eigenvalues are $\alpha_{\parallel, \text{b}} = \alpha_{\perp, \text{b}} = 1$. In this case only the bulk eigenstate gives rise to absorption $I_{\text{b}, \parallel} = V i_{\parallel}$ and $I_{\text{b}, \perp} = V i_{\perp}$, where the two modes

$$i_{\parallel} = \frac{\pi}{4\mu_0} B_z'^2 \chi \Omega^2, \quad (20)$$

$$i_{\perp} = \frac{\pi}{4\mu_0} (B_x^2 + B_y^2) \chi \omega_0^2, \quad (21)$$

and $V = \int d^3r$ is the volume of the liquid.

In the presence of dipole unlocking also other eigenstates contribute to the absorption. Their intensities are given by^{2,9,20}

$$I_{\parallel, k} = i_{\parallel} \alpha_{\parallel, k} Q_{\parallel, k} = i_{\parallel} \alpha_{\parallel, k} \left| \int d^3r \psi_{\parallel, k}(\mathbf{r}) \right|^2, \quad (22)$$

$$I_{\perp, k} = i_{\perp} Q_{\perp, k} = i_{\perp} \left| \int d^3r \psi_{\perp, k}(\mathbf{r}) \exp[i\theta(\mathbf{r})] \right|^2. \quad (23)$$

Here the Q_k 's satisfy the sum rules

$$\sum_{k=0}^{\infty} Q_{\parallel, k} = \sum_{k=0}^{\infty} Q_{\perp, k} = V, \quad (24)$$

$$\sum_{k=0}^{\infty} \alpha_{\parallel, k} Q_{\parallel, k} = \int d^3r U_{\parallel}, \quad (25)$$

$$\sum_{k=0}^{\infty} \alpha_{\perp, k} Q_{\perp, k} = \int d^3r \left[(\hat{\mathbf{l}} \cdot \hat{\mathbf{d}}_0)^2 - l_z^2 \right], \quad (26)$$

$$\sum_{k=0}^{\infty} \alpha_{\parallel, k}^2 Q_{\parallel, k} = \int d^3r U_{\parallel}^2, \quad (27)$$

$$\sum_{k=0}^{\infty} \alpha_{\perp, k}^2 Q_{\perp, k} = \int d^3r \left\{ \left[(\hat{\mathbf{l}} \cdot \hat{\mathbf{d}}_0)^2 - l_z^2 \right]^2 + (\hat{\mathbf{l}} \times \hat{\mathbf{d}}_0)_z^2 (\hat{\mathbf{l}} \cdot \hat{\mathbf{d}}_0)^2 \right\}, \quad (28)$$

and so on. The sum rules can be derived using the orthogonality properties of the eigenfunctions. [In Eq. (28) one also needs Eq. (7).] The lowest-order rules (24)-(26) apparently are equivalent to the sum rules presented by Leggett.²¹

III. EQUILIBRIUM STRUCTURE OF A SPLAY SOLITON

The minimum of the dipole energy (3) can be achieved in two ways: either $\hat{\mathbf{l}}$ and $\hat{\mathbf{d}}$ are parallel or they are antiparallel. This double degeneracy gives rise to domain walls or solitons. On one side of the wall $\hat{\mathbf{l}} = \hat{\mathbf{d}}$ and on the other side $\hat{\mathbf{l}} = -\hat{\mathbf{d}}$. We will study cases where the static field \mathbf{B}_0 is either perpendicular or parallel to the plane of the soliton wall. The soliton structures in these cases are known to have composite twist and splay structures, respectively.⁸ The structure and the fundamental NMR frequency of a twist soliton have been solved analytically.^{2,7,8} Here we concentrate on the case of a splay soliton, which has previously been studied only by variational methods.^{8,9,22,23} Its structure is illustrated in Fig. 1.

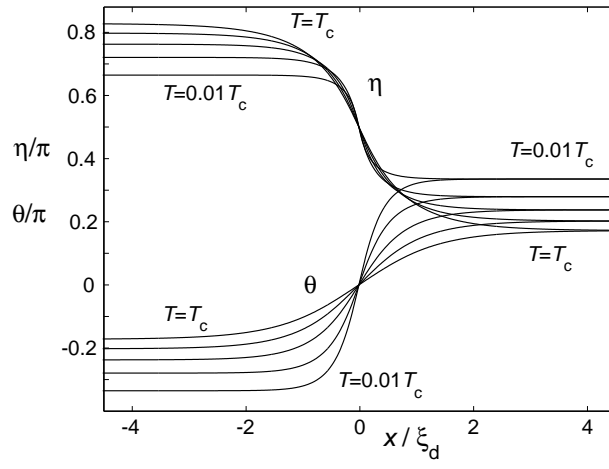


FIG. 2: The functions $\eta(x)$ and $\theta(x)$ for a splay soliton at temperatures $T/T_c = 0.01, 0.25, 0.50, 0.75, 1.00$. The parameter values correspond to weak coupling at 3.4 MPa ($F_1^s = 14.45$ and $F_1^a = -1$).

In the cases of a twist or a splay soliton, both $\hat{\mathbf{l}}$ and $\hat{\mathbf{d}}$ are in the plane perpendicular to \mathbf{B}_0 . We parametrize

$$\hat{\mathbf{l}} = \hat{\mathbf{x}} \cos \eta + \hat{\mathbf{y}} \sin \eta \quad (29)$$

and $\hat{\mathbf{d}}$ as above, Eq. (6). For a splay soliton the angles θ and η are taken as functions of x only. We use the boundary conditions $\eta(+\infty) = \theta(+\infty)$ and $\eta(-\infty) = \theta(-\infty) + \pi$. Substituting the vector fields (6) and (29) into the total energy (2) gives that the energy per unit area is

$$f_s = \frac{1}{2} \int dx [(K_s \sin^2 \eta + K_b \cos^2 \eta) \left(\frac{d\eta}{dx} \right)^2 + (K_6 \sin^2 \eta + K_5 \cos^2 \eta) \left(\frac{d\theta}{dx} \right)^2 - \lambda_d \cos^2(\eta - \theta)] . \quad (30)$$

The energy functional (30) was discretized using equal intervals ($x_i = -L/2 + Li/N$, $i = 0, \dots, N$), and the values of η and θ at these discrete points were taken to be the minimizing variables. The boundary conditions were taken into account by linear initial approximations $\eta = (\pi/2) - (2\pi/3L)x$ and $\theta = (\pi/3L)x$. The minimization can be done by a simple relaxation method. The resulting functions $\eta(x)$ and $\theta(x)$ at different temperatures are shown in Fig. 2.

IV. PRINCIPAL NMR FREQUENCY

We now apply the theory of Sec. II to calculate NMR properties of solitons. For solitons $l_z \equiv 0$, which decouples the longitudinal and transverse modes at arbitrary ω_0 in Eqs. (12). Thus the eigenvalues $\alpha_{\perp,k}$ are related to resonance frequencies as given in Eq. (18) at any field.

The main signature of solitons in the NMR spectrum comes from the lowest eigenvalue of Schrödinger-like equations (15) and (16). This lowest frequency can be calculated, for example, using a variational formulation:

$$\alpha_{\parallel,\perp} = \min_{\psi} \frac{\int d^3r [K_6 |\nabla \psi|^2 + (K_5 - K_6) |\hat{\mathbf{l}} \cdot \nabla \psi|^2 + \lambda_d U_{\parallel,\perp} |\psi|^2]}{\lambda_d \int d^3r |\psi|^2} . \quad (31)$$

This was discretized and the values of $\psi(x_i)$ were taken to be the minimizing variables. The form for the initial approximation used was $\psi(x) = \cosh^n(qx)$ and the boundary conditions $d\psi/dx = 0$ were assumed at the end points. The length L was increased until its effect disappeared. One solution is shown in Fig. 3. In Fig. 4 we plot the temperature dependence of the lowest resonance frequencies as well as some experimental data. For completeness we

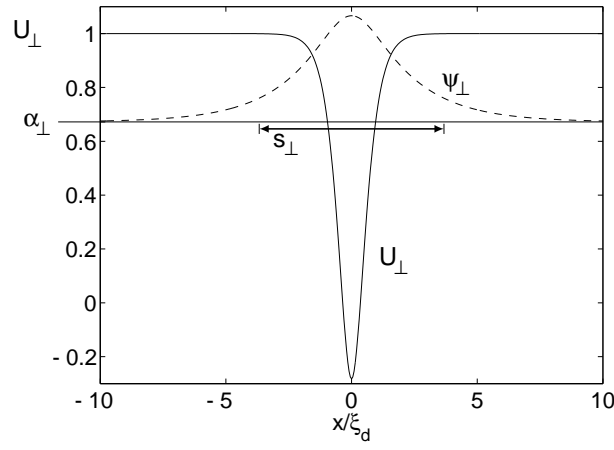


FIG. 3: The potential U_{\perp} (solid line), the lowest eigenvalue α_{\perp} , and the eigenfunction ψ_{\perp} (dashed line, vertical scale arbitrary) for transverse resonance of a splay soliton at $T \approx T_c$. The absorption thickness s_{\perp} gives the effective width of the wave function in NMR.

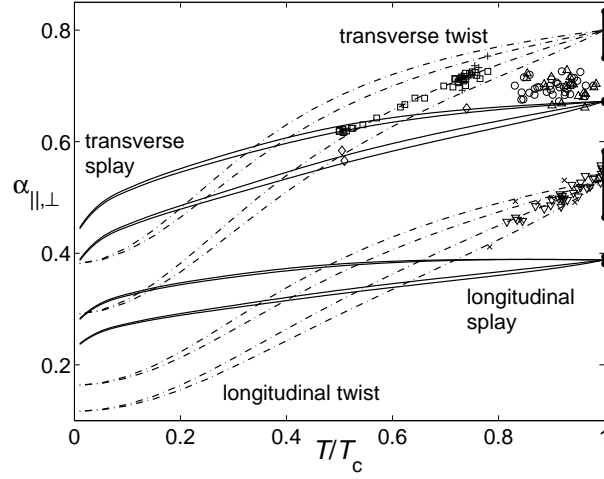


FIG. 4: The reduced resonance frequencies α_{\parallel} (17) and α_{\perp} (18) as functions of temperature. Splay-soliton transverse resonance: four upper solid lines and experimental points \circ (Ref. 6), \triangle (Ref. 10), and \diamond (Ref. 23). Splay-soliton longitudinal resonance: four lower solid lines. Twist-soliton transverse resonance: four upper dash-dotted lines and experimental points $+$ (Ref. 24) and \square (Ref. 23). Twist-soliton longitudinal resonance: four lower dash-dotted lines and experimental points \times (Ref. 5) and ∇ (Ref. 6). In each case there are four theoretical lines, which in order of decreasing α correspond to $F_1^a = 0$ & weak coupling, $F_1^a = 0$ & gap enhancement, $F_1^a = -1$ & weak coupling, and $F_1^a = -1$ & gap enhancement. Good agreement between theory and experiment is achieved with $F_1^a = -1$ and weak coupling except for the high-temperature transverse splay data. The effect of strong-coupling corrections is shown at $T/T_c = 1$ where the lower ends of the bars correspond to $\gamma = 2$ and the upper ends to $\gamma = 4$. The experimental data is plotted with higher resolution in Fig. 10.

also include the analytical results for the twist soliton:^{2,8}

$$\alpha_{\parallel}^{\text{twist}} = \frac{1}{2K_t} [\sqrt{(9K_t + K_6)(K_t + K_6)} - 3K_t - K_6] \quad (32)$$

$$\alpha_{\perp}^{\text{twist}} = \frac{K_6}{K_6 + K_t}. \quad (33)$$

The reduced frequency shifts α_{\parallel} (17) and α_{\perp} (18) depend only on the ratios of the hydrodynamic coefficients K_b , K_s , K_t , K_5 , and K_6 . (Note that the absolute magnitudes of K_i 's and λ_d define length and energy scales that do not affect α_{\parallel} or α_{\perp} .) In the weak-coupling approximation the ratios of K_i 's are functions of an infinite set of Fermi-liquid

parameters F_j^s and F_j^a , with $j = 1, 3, 5$, etc.¹⁶ Here we neglect all the coefficients with $j > 1$ since they are unknown. For F_1^s we use the value by Greywall²⁵ at the melting pressure, $F_1^s = 14.5$. However, the dependence on F_1^s is weak. For example, the variation $F_1^s = 14.5 \pm 1$ shows up only in the fourth decimal of α at $T = 0.8T_c$. In terms of pressure, the maximum difference in α between 2.6 and 3.4 MPa is 1% at temperatures higher than $0.5T_c$. The value $F_1^a = -1$ was taken from Ref. 26 and it is also consistent with Ref. 27. In order to see the effect of F_1^a we also used $F_1^a = 0$. It can be seen in Fig. 4 that this shifts the resonance frequency up at temperatures below T_c .

There are no quantitative calculations of strong-coupling effects in the A phase at a general temperature. In order to get some idea how strong coupling could affect the soliton frequencies, we use a “trivial strong-coupling” model developed by Serene and Rainer²⁸ for the B phase. In this model the weak-coupling energy gap is multiplied by a factor that depends on the temperature and on the jump of the specific heat $\Delta C_B/C_n$ at $T = T_c$. This dependence is tabulated in Ref. 28. We adapt this model to the A phase by calculating the multiplying factor using the same table but substituting $\frac{6}{5}\Delta C_A/C_n$ in place of $\Delta C_B/C_n$, and using extrapolation when needed. We take $\Delta C_A/C_n$ from measurements by Greywall.²⁵ It can be seen in Fig. 4 that the gap enhancement, which affects only intermediate temperatures, has a smaller effect than the change of F_1^a .

In the limiting case $T \rightarrow T_c$ the reduced frequencies α_{\parallel} and α_{\perp} are independent of any parameters appearing in the weak-coupling model, including also the gap enhancement. This is a consequence of the Ginzburg-Landau expansion that gives to the parameters K_i the ratios $K_b : K_s : K_t : K_5 : K_6 = \gamma : 1 : 1 : 2 : (\gamma + 1)$. The only free parameter here is γ , which in the weak coupling (with or without gap enhancement) has the value $\gamma = 3$. This value is changed only when nontrivial strong-coupling corrections are included. The “weak-coupling-plus” model by Serene and Rainer²⁹ gives an estimate $\gamma \approx 3.12$. Figure 4 shows the reduced frequencies corresponding to $\gamma = 2$ and $\gamma = 4$. We see that this variation changes the splay soliton α_{\perp} less than 3% but for the twist soliton the effect is ten times larger.

There is rather good agreement between the experiment and the theory corresponding to weak coupling and $F_1^a = -1$. Equally good agreement is achieved with gap enhancement and $F_1^a \approx -0.7$. The longitudinal twist data is a strong indication that the deviation from the weak-coupling value $\gamma = 3$ is small, as predicted by Serene and Rainer.²⁹ The only major difference between theory and experiment exists in the transverse splay-soliton frequency at high temperatures. It seems very difficult to improve the agreement in this case by any change of the parameters in the theory above since $\alpha_{\perp}^{\text{splay}}$ at T_c is effectively fixed. On the experimental side, one possibility is that the field is not precisely in the plane of the soliton in the measurements. This would add a small twist component to the splay soliton and thus shift up the frequency.⁸ Another possibility is that the inclusion of relaxation mechanisms could shift the calculated resonance frequency, as will be discussed in Sec. VI.

At T_c we find the eigenvalues $\alpha_{\parallel} = 0.388$ and $\alpha_{\perp} = 0.672$ for $\gamma = 3$. These differ slightly from the variational results by Maki and Kumar⁸ that are 0.403 and 0.677, respectively.

V. ABSORPTION AND HIGHER MODES

Here we calculate the intensity of the principal soliton peak and analyze the absorption at other frequencies. For planar objects intensities (22) and (23) are most conveniently expressed in the form of an absorption thickness s_k , which equals Q_k divided by the area of the planar object,

$$s_k = \frac{Q_k}{A}, \quad (34)$$

for each mode k . The absorption thicknesses in the lowest eigenstate are plotted in Fig. 5.

The absorption for a twist soliton can be calculated analytically. Substituting the eigenfunction $\psi = c_1 \text{sech}^{\mu} az$ into Eqs. (22) and (23) and using $\theta = c_2 - \mu_{\perp} \text{sgn}(z) \arccos(\text{sech} az)$ (Refs. 8 and 2) we find

$$s_{\parallel}^{\text{twist}} = \frac{\sqrt{\pi} \Gamma^2(\frac{\mu_{\parallel}}{2}) \Gamma(\mu_{\parallel} + \frac{1}{2})}{a \Gamma(\mu_{\parallel}) \Gamma^2(\frac{\mu_{\parallel} + 1}{2})} \quad (35)$$

$$s_{\perp}^{\text{twist}} = \frac{\sqrt{\pi} 4^{1-\mu_{\perp}} \Gamma(\mu_{\perp})}{a \Gamma(\mu_{\perp} + \frac{1}{2})}. \quad (36)$$

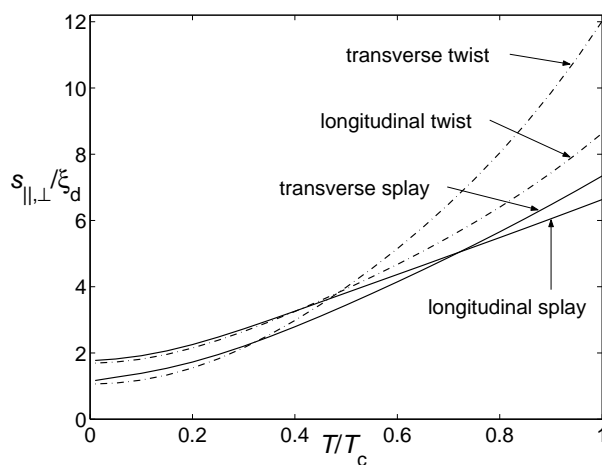


FIG. 5: Absorption (34) of the principal soliton peak in four cases. The parameter values correspond to weak coupling at 3.4 MPa ($F_1^s = 14.45$ and $F_1^a = -1$). The numerical values at T_c are $s_{||}^{\text{splay}} = 6.63\xi_d$, $s_{\perp}^{\text{splay}} = 7.35\xi_d$, $s_{||}^{\text{twist}} = 8.64\xi_d$, and $s_{\perp}^{\text{twist}} = 12.02\xi_d$.

Here Γ is the Gamma function and

$$a = \sqrt{\frac{\lambda_d(K_6 + K_t)}{K_6 K_t}} \quad (37)$$

$$\mu_{||} = \frac{1}{2} \left(\sqrt{\frac{9K_t + K_6}{K_t + K_6}} - 1 \right) \quad (38)$$

$$\mu_{\perp} = \frac{K_t}{K_6 + K_t}. \quad (39)$$

In order to get all the resonance modes, we discretize the space as discussed above ($x_i = -L/2 + Li/N$, $i = 0, \dots, N$, for twist soliton replace x by z). This means that Eqs. (15) and (16) turn into a matrix eigenvalue problem. This can be solved by standard library routines for matrices of reasonable size. This gives all the frequencies, including the fundamental one (31). However, the higher modes extend over the whole interval, and it is important to fix boundary conditions for them. We require zero derivative of ψ at $x = \pm L/2$. This can be justified by considering a lattice of solitons. The general eigenfunctions ψ of Eqs. (15) and (16) are of the Bloch form, but only strictly periodic functions lead to nonzero absorption in Eqs. (22) and (23). The unit cell of a soliton lattice $x = -L/2, \dots, 3L/2$ consists of two solitons located around $x = 0$ and $x = L$. The vectors $\hat{\mathbf{l}}$ and $\hat{\mathbf{d}}$ have the symmetries $\hat{\mathbf{l}}(L/2 + x) = \hat{\mathbf{l}}(L/2 - x)$ and $\hat{\mathbf{d}}(L/2 + x) = \hat{\mathbf{d}}(L/2 - x)$. This implies that the eigenfunctions can be classified as symmetric or antisymmetric (with respect to $x = L/2$). The symmetric solutions have $d\psi/dx(\pm L/2) = 0$, and the antisymmetric solutions can be neglected since they do not contribute to the absorption.

The results for the frequencies and intensities of the higher modes are shown in Fig. 6. As expected, the higher modes depend on the size L of the system used in the calculation. The modes seem to appear as pairs above the bulk peak. The bulk peak also seems to consist of two peaks that do not appear exactly at $\alpha = 1$ due to finite L . In fact, the finite L corresponds to a periodic lattice of solitons, which should give rise to peaks that are analogous to the Bragg peaks in the x-ray scattering from periodic solids. Such peaks are indeed seen experimentally in the case of a vortex sheet, where a nearly periodic arrangement is automatically generated.³⁰ The observation of the peaks depends essentially on dissipative effects, which broadens the peaks. This will be discussed in the following section.

VI. THE EFFECT OF DISSIPATION

There are two sources of dissipation that are important for solitons. The nonequilibrium between normal and superfluid magnetizations is the main relaxation mechanism in homogeneous superfluid ^3He .^{31,32,33} In inhomogeneous situations the nonequilibrium between normal magnetizations at different locations causes relaxation via spin diffusion. We study these two mechanisms below, the latter in the case where the inhomogeneity arises from the soliton. We

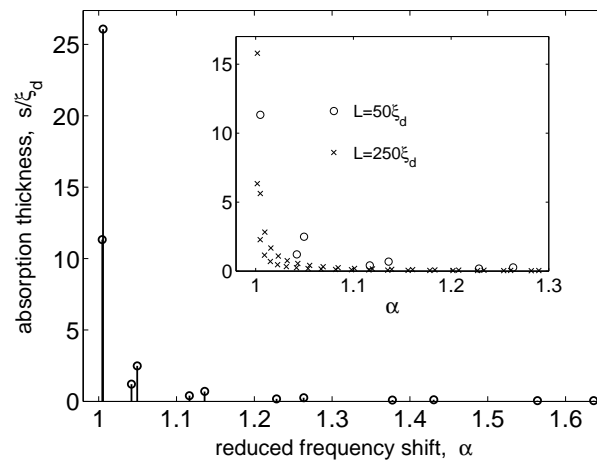


FIG. 6: The higher modes in the case of transverse resonance of a splay soliton. The length used in the calculation is $L = 50\xi_d$ in the main frame whereas the inset also contains the points for $L = 250\xi_d$. In both cases the lattice spacing of the discretized lattice is $0.1\xi_d$. Other parameters are weak coupling at 3.4 MPa ($F_1^s = 14.45$, $F_1^a = -1$) and temperature $T = 0.95T_c$.

neglect extrinsic effects such as the inhomogeneity caused by nonuniform magnetic field. We also do not consider dissipation caused by orbital motion. According to the estimation in Ref. 19, this is important only at temperatures very near T_c , region which is vanishingly small on the scale of Fig. 4.

Our treatment of the dissipation is purely phenomenological. For normal-superfluid relaxation we use the model developed by Leggett and Takagi, which is extensively described in Ref. 33. For the relaxation of spatially nonequilibrium magnetization we use simple diffusion equation. This approach can be correct only when the mean free path of the quasiparticles is smaller than the thickness of the soliton, and therefore it necessarily fails at low temperatures, where the mean free path diverges. Our treatment also neglects the tensor character of the spin-diffusion coefficient, as well as the anisotropic energy gap with varying anisotropy axis $\hat{\mathbf{l}}(\mathbf{r})$, which leads to Andreev reflection of the quasiparticles.

In order to treat the relaxation, the spin polarization \mathbf{S} is divided into a superfluid (pair) part \mathbf{S}_p and a normal (quasiparticle) part $\mathbf{S}_q = \mathbf{S} - \mathbf{S}_p$. Both parts have separate equations of motion

$$\dot{\mathbf{S}}_q = \gamma \mathbf{S}_q \times \left(\mathbf{B} - \mu_0 \gamma \frac{F_0^a}{\chi_0} \mathbf{S}_p \right) + \frac{1}{\tau} [(1 - \lambda) \mathbf{S}_p - \lambda \mathbf{S}_q] + \kappa \nabla^2 \mathbf{S}_q \quad (40a)$$

$$\dot{\mathbf{S}}_p = \gamma \mathbf{S}_p \times \left(\mathbf{B} - \mu_0 \gamma \frac{F_0^a}{\chi_0} \mathbf{S}_q \right) - \frac{1}{\tau} [(1 - \lambda) \mathbf{S}_p - \lambda \mathbf{S}_q] - \hat{\mathbf{d}} \times \frac{\delta f}{\delta \hat{\mathbf{d}}} \quad (40b)$$

$$\dot{\hat{\mathbf{d}}} = \gamma \hat{\mathbf{d}} \times \left[\mathbf{B} - \mu_0 \gamma \frac{F_0^a}{\chi_0} \mathbf{S}_q - \mu_0 \gamma \left(\frac{F_0^a}{\chi_0} + \frac{1}{\lambda \chi_0} \right) \mathbf{S}_p \right]. \quad (40c)$$

Except the spin-diffusion term $\kappa \nabla^2 \mathbf{S}_q$, these equations are the same as in Ref. 33. Here χ_0 is the susceptibility in the absence of Fermi-liquid effects. As above, χ is the susceptibility in the normal state, so that $\chi/\chi_0 = 1/(1 + F_0^a)$. The function $\lambda(T/T_c)$ is defined as the equilibrium fraction of the superfluid magnetization, and is given by Eq. (4.23) in Ref. 33. The Leggett-Takagi relaxation time τ describes local relaxation of \mathbf{S}_p and \mathbf{S}_q to their equilibrium values. The spin diffusion appears via term $\kappa \nabla^2 \mathbf{S}_q$ in the equation for $\dot{\mathbf{S}}_q$ (40a). In the normal state the spin-diffusion constant κ is related to the spin-diffusion time τ_D by³⁴

$$\kappa = \frac{1}{3} v_F^2 (1 + F_0^a) \tau_D, \quad (41)$$

where v_F is the Fermi velocity. We use this parametrization also in the superfluid state. Note that κ is defined as the spin-diffusion constant for \mathbf{S}_q , so that the effective diffusion constant for the total magnetization \mathbf{S} is $(1 - \lambda)\kappa$.

We continue by writing the equations for variables $\hat{\mathbf{d}}$, \mathbf{S} , and the deviation from local equilibrium

$$\boldsymbol{\eta} = \mathbf{S}_p - \lambda \mathbf{S}. \quad (42)$$

Similarly, as in Sec. II, we linearize the equations and assume harmonic time dependence. We use the fact that $l_z = 0$ in solitons. As a consequence, the transverse and longitudinal modes separate at any field B_0 . Differing from Sec.

If we introduce dimensionless quantities by defining $S^\pm = (\Omega^2/\lambda_d\omega_0)(S'_x \pm iS'_y)$ and $\eta^\pm = (\Omega^2/\lambda_d\omega_0)(\eta'_x \pm i\eta'_y)$. For transverse oscillations we get the equations

$$\frac{\omega}{\omega_0} S^\pm = \left[\pm 1 + i(1 - \lambda) \frac{\kappa}{\omega_0} \nabla^2 \right] S^\pm - i \frac{\kappa}{\omega_0} \nabla^2 \eta^\pm \mp \frac{\Omega^2}{\omega_0^2} e^{\pm i\theta} (\mathcal{D} + U_\perp) d_z \mp \frac{B_\pm}{B_0}, \quad (43a)$$

$$\begin{aligned} \frac{\omega}{\omega_0} \eta^\pm &= \left(\pm \frac{1}{1 + F_0^a} - \frac{i}{\omega_0 \tau} + i\lambda \frac{\kappa}{\omega_0} \nabla^2 \right) \eta^\pm - i\lambda(1 - \lambda) \frac{\kappa}{\omega_0} \nabla^2 S^\pm \\ &\mp (1 - \lambda) \frac{\Omega^2}{\omega_0^2} e^{\pm i\theta} (\mathcal{D} + U_\perp) d_z, \end{aligned} \quad (43b)$$

$$\begin{aligned} \frac{\omega}{\omega_0} d_z &= \frac{1}{2} (S^- e^{i\theta} - S^+ e^{-i\theta}) + \frac{\chi}{2\lambda\chi_0} (\eta^- e^{i\theta} - \eta^+ e^{-i\theta}) \\ &+ \frac{1}{2B_0} (B_+ e^{-i\theta} - B_- e^{i\theta}). \end{aligned} \quad (43c)$$

The full solution of this problem can be written as a five-component vector $\psi = (S^- \ \eta^- \ d_z \ \eta^+ \ S^+)^T = \sum_i c_i \psi_i$, where the ψ_i 's satisfy the homogeneous equation where $B_\pm = 0$. The eigenvalues ω_i of the homogeneous equation are now complex valued, and the eigenvectors ψ_i are not orthogonal to each other. In order to solve for the absorption spectrum we find that the following adjoint eigenvalue problem:³⁵

$$\frac{\omega}{\omega_0} \underline{S}^\pm = \left[\pm 1 + i(1 - \lambda) \frac{\kappa}{\omega_0} \nabla^2 \right] \underline{S}^\pm - i\lambda(1 - \lambda) \frac{\kappa}{\omega_0} \nabla^2 \underline{\eta}^\pm \mp \frac{1}{2} e^{\mp i\theta} \underline{d}_z \quad (44a)$$

$$\frac{\omega}{\omega_0} \underline{\eta}^\pm = \left(\pm \frac{1}{1 + F_0^a} - \frac{i}{\omega_0 \tau} + i\lambda \frac{\kappa}{\omega_0} \nabla^2 \right) \underline{\eta}^\pm - i \frac{\kappa}{\omega_0} \nabla^2 \underline{S}^\pm \mp \frac{\chi}{2\lambda\chi_0} e^{\mp i\theta} \underline{d}_z \quad (44b)$$

$$\frac{\omega}{\omega_0} \underline{d}_z = \frac{\Omega^2}{\omega_0^2} (\mathcal{D} + U_\perp) [e^{-i\theta} \underline{S}^- - e^{i\theta} \underline{S}^+ + (1 - \lambda)(e^{-i\theta} \underline{\eta}^- - e^{i\theta} \underline{\eta}^+)] \quad (44c)$$

has the same eigenvalues ω_i as the homogeneous version of problem (43) and that the eigenvectors $\underline{\psi}_i = (\underline{S}_i^- \ \underline{\eta}_i^- \ \underline{d}_{z,i} \ \underline{\eta}_i^+ \ \underline{S}_i^+)^T$ are orthogonal to ψ_j 's:

$$\int \underline{\psi}_i^T \psi_j d^3r = \delta_{ij}. \quad (45)$$

When deriving this we have assumed zero derivate for the wave functions far from the soliton by considering a lattice of solitons as was discussed in Sec. V. The power absorption can now be written as

$$\begin{aligned} P(\omega) &= \frac{1}{2} \gamma \omega \int \text{Im} (\mathbf{B}' \cdot \mathbf{S}') d^3r \\ &= \frac{\chi B_0 \omega}{4\mu_0} \sum_j \text{Im} \left[c_j \int d^3r (B_-^* S_j^- + B_+^* S_j^+) \right], \end{aligned} \quad (46)$$

where the coefficients c_j are given by

$$c_j = \frac{\gamma}{\omega - \omega_j} \int d^3r \left[B_- \underline{S}_j^- - B_+ \underline{S}_j^+ + \frac{1}{2} (e^{-i\theta} B_+ - e^{i\theta} B_-) \underline{d}_{z,j} \right]. \quad (47)$$

We observe that the eigenfunctions are not symmetric with respect to the center of the soliton. This apparently is caused by the spin-diffusion term.

In the hydrodynamic limit where $\omega\tau \ll 1$ one may solve η^\pm from Eq. (43) and to linear order in τ

$$\eta^\pm = -\tau\lambda(1 - \lambda)\kappa\nabla^2 S^\pm \pm i\tau(1 - \lambda) \frac{\Omega^2}{\omega_0} e^{\pm i\theta} (\mathcal{D} + U) d_z. \quad (48)$$

If we additionally ignore the term $\nabla^2 \eta^\pm$, the equations for the three-component vector $(S^- \ d_z \ S^+)^T$ read

$$\frac{\omega}{\omega_0} S^\pm = \left[\pm 1 + i(1 - \lambda) \frac{\kappa}{\omega_0} \nabla^2 \right] S^\pm \mp \frac{\Omega^2}{\omega_0^2} e^{\pm i\theta} (\mathcal{D} + U_\perp) d_z \mp \frac{B_\pm}{B_0}, \quad (49a)$$

$$\begin{aligned} \frac{\omega}{\omega_0} d_z &= \frac{1}{2} e^{i\theta} \left[1 - \frac{\tau\chi(1 - \lambda)\kappa}{\chi_0} \nabla^2 \right] S^- - \frac{1}{2} e^{-i\theta} \left[1 - \frac{\tau\chi(1 - \lambda)\kappa}{\chi_0} \nabla^2 \right] S^+ \\ &- i \frac{\tau\chi\Omega^2(1 - \lambda)}{\chi_0\omega_0\lambda} (\mathcal{D} + U_\perp) d_z + \frac{1}{2B_0} (B_+ e^{-i\theta} - B_- e^{i\theta}). \end{aligned} \quad (49b)$$

The homogeneous adjoint problem for this is given by

$$\frac{\omega}{\omega_0} \underline{S}^\pm = \left[\pm 1 + i(1 - \lambda) \frac{\kappa}{\omega_0} \nabla^2 \right] \underline{S}^\pm \mp \frac{1}{2} \left(1 - \frac{\tau \chi (1 - \lambda) \kappa}{\chi_0} \nabla^2 \right) (e^{\mp i\theta} \underline{d}_z), \quad (50a)$$

$$\frac{\omega}{\omega_0} \underline{d}_z = \frac{\Omega^2}{\omega_0^2} (\mathcal{D} + U_\perp) (e^{-i\theta} \underline{S}^- - e^{i\theta} \underline{S}^+) - i \frac{\tau \chi \Omega^2 (1 - \lambda)}{\chi_0 \omega_0 \lambda} (\mathcal{D} + U_\perp) \underline{d}_z. \quad (50b)$$

The equation for the power absorption does not need any modifications. One must be careful since the validity region of the hydrodynamic approximation is not very large. For temperatures near T_c one must, for typical values of τ , have $B_0 \lesssim 15$ mT. We mainly used the hydrodynamic approximation for checking our calculations in the limit of $\tau \rightarrow 0$.

For longitudinal case, where $\mathbf{B}' = B' \hat{\mathbf{z}} \parallel \mathbf{B}_0$, we also define dimensionless quantities by writing $\mathbf{S}' = \hat{\mathbf{z}} \lambda_d S_z / \Omega$, $\boldsymbol{\eta}' = \hat{\mathbf{z}} \lambda_d \eta_z / \Omega$, and $\mathbf{d}' = d_\theta \hat{\mathbf{z}} \times \hat{\mathbf{d}}_0$. The equations of motions are

$$\frac{\omega}{\Omega} S_z = i(1 - \lambda) \frac{\kappa}{\Omega} \nabla^2 S_z - i \frac{\kappa}{\Omega} \nabla^2 \eta_z - i(\mathcal{D} + U_\parallel) d_\theta, \quad (51a)$$

$$\frac{\omega}{\Omega} \eta_z = -i\lambda(1 - \lambda) \frac{\kappa}{\Omega} \nabla^2 S_z - i \left(\frac{1}{\tau \Omega} - \lambda \frac{\kappa}{\Omega} \nabla^2 \right) \eta_z - i(1 - \lambda)(\mathcal{D} + U_\parallel) d_\theta, \quad (51b)$$

$$\frac{\omega}{\Omega} d_\theta = i \left(S_z + \frac{\chi \eta_z}{\lambda \chi_0} \right) - i \frac{\gamma B'}{\Omega}, \quad (51c)$$

and the homogeneous adjoint problem for this is given by

$$\frac{\omega}{\Omega} \underline{S}_z = i(1 - \lambda) \frac{\kappa}{\Omega} \nabla^2 \underline{S}_z - i\lambda(1 - \lambda) \frac{\kappa}{\Omega} \nabla^2 \underline{\eta}_z + i \underline{d}_\theta, \quad (52a)$$

$$\frac{\omega}{\Omega} \underline{\eta}_z = -i \frac{\kappa}{\Omega} \nabla^2 \underline{S}_z - i \left(\frac{1}{\tau \Omega} - \lambda \frac{\kappa}{\Omega} \nabla^2 \right) \underline{\eta}_z + i \frac{\chi}{\lambda \chi_0} \underline{d}_\theta, \quad (52b)$$

$$\frac{\omega}{\Omega} \underline{d}_\theta = -i(\mathcal{D} + U_\parallel) [\underline{S}_z + (1 - \lambda) \underline{\eta}_z]. \quad (52c)$$

Power absorption for longitudinal case is given by

$$P(\omega) = \frac{\chi \Omega \omega}{2\mu_0 \gamma} \sum_j \text{Im} \left(c_j \int B'^* S_{z,j} d^3 r \right), \quad (53)$$

where the c_j 's are the coefficients of the full solution $\psi = (S_z \eta_z d_\theta)^T = \sum_j c_j (S_{z,j} \eta_{z,j} d_{\theta,j})^T$ and given by

$$c_j = \frac{i\gamma B'}{\omega_j - \omega} \int \underline{d}_{\theta,j} d^3 r. \quad (54)$$

Similar to the transverse case one could write the hydrodynamic equations using only d_θ and S_z .

The numerical solution for these different eigenvalue problems is obtained by dividing the calculation length $x = -L/2, \dots, L/2$, for example, to 1000 points and approximating the spatial derivatives by differences. The eigenvalues and vectors of the resulting sparse 5000×5000 (or in the longitudinal case 3000×3000) matrix A are then solved by MATLAB. We make use of sparse matrices and calculate normally only 20 lowest eigenvalues with $\text{Re}[\omega_k] > 0$ that give the main contribution to the absorption spectrum. The complex mode frequencies ω_k are related to the reduced frequency shifts α_k as given by Eqs. (17) and (18).

Additional parameters appear in the calculation compared to the dissipationless case. The most crucial ones are the relaxation times τ and τ_D . The Leggett-Takagi time τ can be extracted from the width of the bulk peak. Measurements of longitudinal and transverse resonances are in good agreement.³⁶ We have reanalyzed the data by Gully *et al.*³⁶ including strong-coupling corrections as described in Sec. IV and get the fit $\tau = [1.70 + 6.71(1 - T/T_c)](1 + F_0^a)10^{-7}$ s in the range of $T/T_c = 0.78$ – 0.98 . We fix $F_0^a = -0.746$. For the spin-diffusion coefficient κ we use the value $\kappa T^2 = 1.1 \times 10^{-5}$ mK²/s from Refs. 37 and 38. This corresponds to the spin-diffusion time $\tau_D = 1.25 \times 10^{-7} T^{-2}$ mK² s. A few absorption spectra are plotted in Figs. 7–9.

The effect of the normal-superfluid relaxation seems to be simple line broadening. In the transverse resonance the linewidth measured on the α_\perp scale is inversely proportional to the magnetic field B_0 for $B_0 \gg B_d$. This is caused by $i/(\omega_0 \tau)$ term in Eq. (43b). There is no field dependence in the longitudinal resonance since Eqs. (51) do not contain ω_0 . In the longitudinal case the linewidth on the α scale has no strong temperature dependence and approaches a finite constant when $T \rightarrow T_c$. In the transverse case the linewidth on the α scale vanishes as $T \rightarrow T_c$. All these characteristics are the same as predicted for the bulk peaks.

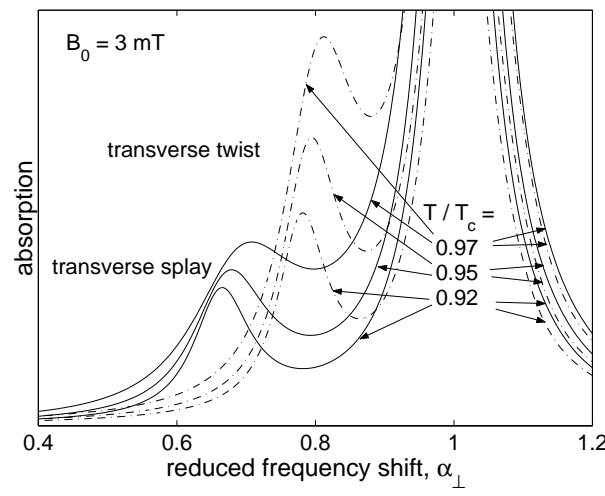


FIG. 7: Absorption spectra for transverse twist soliton (dash-dotted lines) and splay soliton (solid lines) at $T/T_c = 0.92, 0.95$, and 0.97 when $L = 50\xi_d$, $B_0 = 3$ mT, $\tau = [1.70 + 6.71(1 - T/T_c)](1 + F_0^a)10^{-7}$ s, and $\tau_D = 1.25 \times 10^{-7}T^{-2}$ mK² s. Other parameters are obtained using weak coupling and pressure of 3.4 MPa with $F_1^a = -1$ and $F_0^a = -0.746$.

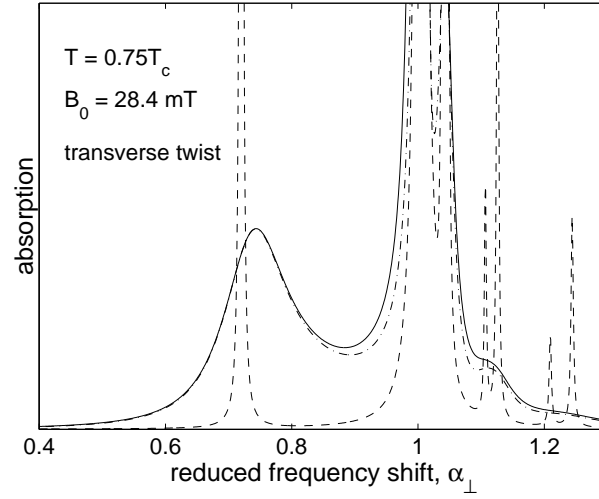


FIG. 8: Transverse absorption spectrum for a twist soliton at $T = 0.75T_c$ and $B_0 = 28.4$ mT (solid line). Other parameters are the same as in Fig. 7. The effect of the two dissipation mechanisms is demonstrated by setting $\tau = 0$ (dash-dotted line) and $\tau_D = 0$ (dashed line).

The effect of spin diffusion is more complicated. In addition to broadening, it shifts the principal soliton peak to higher frequencies. Since the spin diffusion is due to inhomogeneous texture, its strength in the transverse case is obtained by comparing the term $i(1 - \lambda)(\kappa/\omega_0)\nabla^2 S^\pm$ with the term $(\Omega^2/\omega_0^2)\exp(\pm i\theta)(\mathcal{D} + U_\perp)d_z$ in Eq. (43a). Therefore, the effective diffusion constant $\kappa_{\text{eff}}^\perp = (1 - \lambda)\kappa\omega_0/\Omega^2$ is linearly proportional to the magnetic field. As a consequence also the reduced frequency α_\perp of the satellite peak is field dependent. When $B_0 = 5$ mT the effect of diffusion is already quite large at $T = 0.95T_c$ and the soliton satellite peak is almost smeared out. In the longitudinal case there is no field dependence and the effective diffusion constant reduces to $\kappa_{\text{eff}}^\parallel = (1 - \lambda)\kappa/\Omega$. In both transverse and longitudinal cases the effective diffusion coefficients $\kappa_{\text{eff}}^\parallel$ and $\kappa_{\text{eff}}^\perp$ diverge when $T \rightarrow T_c$, as $\Omega \rightarrow 0$.

The relative contributions of normal-superfluid relaxation and spin diffusion are illustrated in Figs. 8 and 9, where both are separately shut off by setting $\tau = 0$ or $\tau_D = 0$. It can be seen that the broadening of the longitudinal satellite peak is mostly caused by normal-superfluid conversion at $T = 0.95T_c$. In the transverse case at high field the spin diffusion becomes the dominant relaxation mechanism, as well as approaching T_c . In uniform order parameter the width of the bulk peak comes solely from normal-superfluid relaxation. Our soliton lattice has many higher peaks in

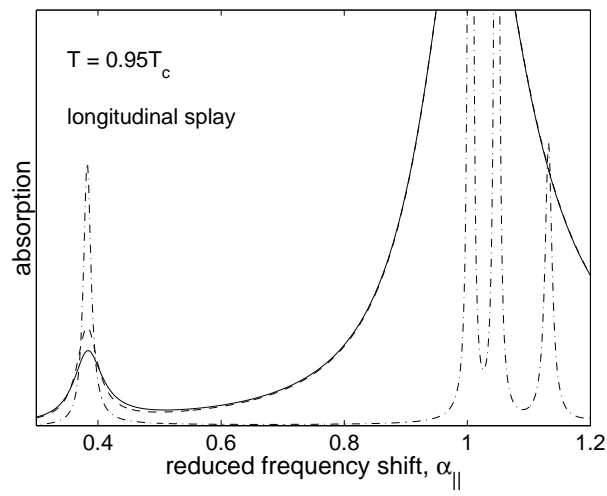


FIG. 9: Longitudinal absorption spectrum for a splay soliton at $T = 0.95T_c$ (solid line). There is no dependence on the magnetic field, and other parameters are the same as in Fig. 7. The effect of the two dissipation mechanisms is demonstrated by setting $\tau = 0$ (dash-dotted line) and $\tau_D = 0$ (dashed line).

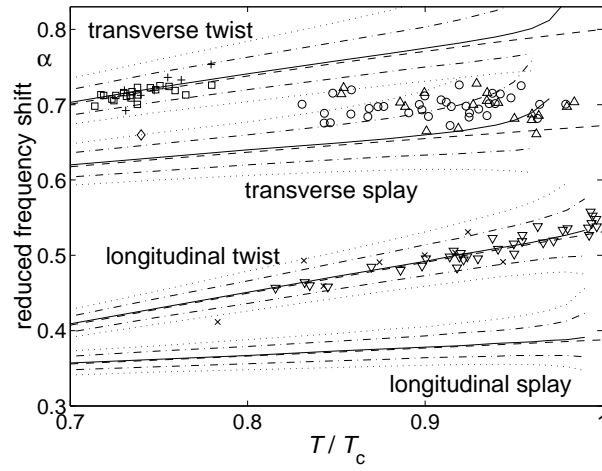


FIG. 10: The resonance frequencies and linewidths as a function of temperature at $B_0 = 3$ mT. The solid lines give the frequency of maximum satellite absorption, the dash-dotted lines 75%, and dotted lines 50% of the maximum. The dashed lines give resonance frequency in the absence of dissipation. Other parameters are $L = 50\xi_d$, $\tau = [1.70 + 6.71(1 - T/T_c)](1 + F_0^a)10^{-7}$ s, $\tau_D = 1.25 \times 10^{-7} T^{-2}$ mK² s, pressure 3.4 MPa ($F_1^s = 14.45$, $F_1^a = -1$, and $F_0^a = -0.746$ and weak coupling). The experimental points are the same as in Fig. 4.

the absence of dissipation, but dissipation seems to remove them. Note that the higher peaks are mostly suppressed by spin diffusion in the case of Fig. 8 but by normal-superfluid relaxation in the case of Fig. 9.

The relatively high field in Fig. 8 has been chosen to allow a comparison to the spectrum of Hakonen *et al.*²⁴ The shape of the twist-soliton spectra are very similar even if the temperature is quite low, where our modeling of the spin diffusion is under suspect. Further spectra at lower field are shown by Parts *et al.*²³ The comparison to Ref. 10 is a different case. In this experiment such a dense soliton lattice was created that no bulk peak was observable. Avenel *et al.*⁵ and Gould and Lee⁶ show soliton spectra measured by sweeping temperature. In all cases a proper comparison to our calculations would require first estimation of the density of solitons and then correcting our calculations for that density, which we have not done. What we can state that there seems to be no obvious contradictions between theory and experiment concerning the linewidth.

A summary of our results at $B_0 = 3$ mT is shown Fig. 10. We see that the frequency of maximum absorption is shifted towards higher frequencies, especially at temperatures near T_c . This alleviates the disagreement found between dissipationless theory and the experiment by Gould and Lee⁶ in the transverse mode of splay soliton. However, the

experimental data does not show any sign of the divergence at T_c predicted by our model. The shift of the resonance frequency results from spin diffusion. For the longitudinal mode it is field independent, but for the transverse mode it increases with increasing field. In high field this shift can be substantial even at $T \approx 0.7T_c$, see Fig. 8. This poses a problem since no field-dependent shift has been observed experimentally. This is the case particularly for the transverse mode of twist soliton measured at $B_0 = 9.9$ mT (\square) (Ref. 23) and 28 mT (+) (Ref. 24). Similar evidence for transverse mode of splay soliton measured at 2.5...3.7 mT (\circ) (Ref. 6) and at 15...20 mT (\triangle) (Ref. 10) is not so clear since the latter data is measured under different conditions, as discussed above.

VII. CONCLUSIONS

The frequencies of soliton satellite peaks in the NMR spectrum are calculated at all temperatures. The agreement of dissipationless theory with experiments is very good. However, there is a small difference in the transverse-mode frequency of a splay soliton near T_c . This difference is partly explained by taking into account spin diffusion. The spin diffusion shifts up the reduced frequencies α at high fields, which has not been observed experimentally. We hope that new experiments could clarify this problem. We also point out the relatively narrow longitudinal line of the splay soliton, which has not been studied experimentally.

It would be of interest to extend the present calculations to vortex lines in $^3\text{He-A}$. This requires two-dimensional calculation and thus would be computationally much more demanding than the present one.

ACKNOWLEDGMENTS

We thank Pete Sivonen for contribution in early stages of this work. This research was supported by the Academy of Finland and the Väisälä foundation.

-
- ¹ A.J. Leggett, Ann. Phys. (N.Y.) **85**, 11 (1974).
 - ² D. Vollhardt and P. Wölfle, *The Superfluid Phases of Helium 3* (Taylor&Francis, London, 1990).
 - ³ G.E. Volovik, *Exotic Properties of Superfluid ^3He* (World Scientific, Singapore, 1992).
 - ⁴ O.V. Lounasmaa and E.V. Thuneberg, Proc. Natl. Acad. Sci. U.S.A. **96**, 7760 (1999).
 - ⁵ O. Avenel, M.E. Bernier, E.J. Varoquaux, and C. Vibet, in *Proceedings of the 14th International Conference on Low Temperature Physics*, edited. M. Krusius and M. Vuorio (North-Holland, Amsterdam, 1975), Vol. 5, p. 429.
 - ⁶ C.M. Gould and D.M. Lee, Phys. Rev. Lett. **37**, 1223 (1976).
 - ⁷ K. Maki and P. Kumar, Phys. Rev. B **16**, 182 (1977).
 - ⁸ K. Maki and P. Kumar, Phys. Rev. B **17**, 1088 (1978).
 - ⁹ R. Bruinsma and K. Maki, Phys. Rev. B **20**, 984 (1979).
 - ¹⁰ C.M. Gould, T.J. Bartolac, and H.M. Bozler, J. Low Temp. Phys. **39**, 291 (1980).
 - ¹¹ G.A. Kharadze and K. Maki, Phys. Rev. B **26**, 1182 (1982).
 - ¹² M. Nakahara and K. Maki, Phys. Rev. B **27**, 4456 (1983).
 - ¹³ A.J. Leggett, Rev. Mod. Phys. **47**, 331 (1975).
 - ¹⁴ M.C. Cross, J. Low Temp. Phys. **21**, 525 (1975).
 - ¹⁵ A.L. Fetter, in *Progress in Low Temperature Physics*, edited by D.F. Brewer (Elsevier, Amsterdam 1986), Vol. X, p. 1.
 - ¹⁶ M. Dörfle, Phys. Rev. B **24**, 6336 (1981).
 - ¹⁷ J.R. Hook, in *Helium Three*, edited by W.P. Halperin and L.P. Pitaevskii (Elsevier, Amsterdam 1990), p. 135.
 - ¹⁸ See <http://boojum.hut.fi/research/theory/qc/bcsgap.html>.
 - ¹⁹ A.J. Leggett and S. Takagi, Ann. Phys. (N.Y.) **110**, 353 (1978).
 - ²⁰ V.Z. Vulovic, D.L. Stein, and A.L. Fetter, Phys. Rev. B **29**, 6090 (1984).
 - ²¹ A.J. Leggett, J. Phys. C **6**, 3187 (1973).
 - ²² D. Vollhardt and K. Maki, Phys. Rev. B **20**, 963 (1979).
 - ²³ Ü. Parts, V.M.H. Ruutu, J.H. Koivuniemi, M. Krusius, E.V. Thuneberg, and G.E. Volovik, Physica B **210**, 311 (1995).
 - ²⁴ P.J. Hakonen, O.T. Ikkala, S.T. Islander, O.V. Lounasmaa, and G.E. Volovik, J. Low Temp. Phys. **53** 425 (1983).
 - ²⁵ D.S. Greywall, Phys. Rev. B **33**, 7520 (1986).
 - ²⁶ D.S. Greywall, Phys. Rev. B **27**, 2747 (1983).
 - ²⁷ D. Candela, N. Masuhara, D.S. Sherrill, and D.O. Edwards, J. Low Temp. Phys. **63**, 369 (1986).
 - ²⁸ J.W. Serene and D. Rainer, Phys. Rep. **101**, 221 (1983).
 - ²⁹ J.W. Serene and D. Rainer, Phys. Rev. B **17**, 2901 (1978).
 - ³⁰ Ü. Parts, J.H. Koivuniemi, M. Krusius, V.M.H. Ruutu, E.V. Thuneberg, and G.E. Volovik, Pis'ma Zh. Eksp. Teor. Fiz. **59**, 816 (1994) [JETP Lett. **59**, 851 (1994)].

- ³¹ R. Combescot and H. Ebisawa, Phys. Rev. Lett. **33**, 810 (1974).
- ³² R. Combescot, Phys. Rev. B **13**, 126 (1976).
- ³³ A.J. Leggett and S. Takagi, Ann. Phys. (N.Y.) **106**, 79 (1977).
- ³⁴ A.J. Leggett, J. Phys. C **3**, 448 (1970).
- ³⁵ P.M. Morse and H. Feshbach, *Methods of Theoretical Physics, Part 1* (McGraw-Hill, New York 1953), p. 884.
- ³⁶ W.J. Gully, C.M. Gould, R.C. Richardson, and D.M. Lee, J. Low Temp. Phys. **24**, 563 (1976).
- ³⁷ A.S. Sachrajda, D.F. Brewer, and W.S. Truscott, J. Low Temp. Phys. **56**, 617 (1984).
- ³⁸ C.J. Pethick, H. Smith, and P. Bhattacharyya, Phys Rev. B **15**, 3384 (1977).